Preprints.org

Article

Not peer-reviewed version

Vision-Based Deformation Monitoring and Risk Analysis of Adjacent High-Speed Railway Piers Under Full Construction Process of New Bridges

Xuena Jia , Liang Xu * , Fengkun Cui , Xingyu Wang , Jin Yao

Posted Date: 27 April 2026

doi: 10.20944/preprints202604.1841.v1

Keywords: high-speed railway; adjacent construction; pier deformation; risk assessment; digital image correlation (DIC); structural health monitoring

Preprints.org is a free multidisciplinary platform providing preprint service that is dedicated to making early versions of research outputs permanently available and citable. Preprints posted at Preprints.org appear in Web of Science, Crossref, Google Scholar, Scilit, Europe PMC, OpenAlex.

Copyright: This open access article is published under a Creative Commons CC BY 4.0 license, which permit the free download, distribution, and reuse, provided that the author and preprint are cited in any reuse.

Preprints.org (www.preprints.org) | NOT PEER-REVIEWED | Posted: 27 April 2026 doi:10.20944/preprints202604.1841.v1

Disclaimer/Publisher's Note: The statements, opinions, and data contained in all publications are solely those of the individual author(s) and contributor(s) and not of MDPI and/or the editor(s). MDPI and/or the editor(s) disclaim responsibility for any injury to people or property resulting from any ideas, methods, instructions, or products referred to in the content.

Article

Vision-Based Deformation Monitoring and Risk Analysis of Adjacent High-Speed Railway Piers Under Full Construction Process of New Bridges

Xuena Jia [1,2], Liang Xu [3,4,*], Fengkun Cui [1], Xingyu Wang [1] and Jin Yao [5]

[1] School of Transportation and Civil Engineering, Shandong Jiaotong University, Jinan 250357, China
[2] State Key Laboratory of Tunnel Engineering, China University of Mining and Technology (Beijing), Beijing 100083, China
[3] Department of Civil Engineering, Suzhou University of Science and Technology, Suzhou 250001, China
[4] State Key Laboratory of Mountain Bridge and Tunnel Engineering, Chongqing Jiaotong University, Chonqing 400030, China
[5] Jiangsu Building Science & Technology Institute Co., Ltd, Suzhou 250001, China
* Correspondence: liangxu360427@usts.edu.cn

Abstract

The proliferation of high-speed railway (HSR) networks necessitates frequent construction activities adjacent to operational lines, posing significant risks to the structural integrity and safety of existing infrastructure. This study addresses the critical need for a comprehensive framework to assess and monitor the deformation of HSR piers throughout the entire construction process of a new, nearby bridge, which includes the cumulative effects of both substructure and superstructure construction. A hybrid methodology integrating quantitative risk assessment and real-time, non-contact monitoring was developed and implemented. A risk evaluation model was established using the Analytic Hierarchy Process (AHP) to structure the problem, combined with Triangular Fuzzy Numbers to handle the inherent uncertainties in expert judgments. The Fuzzy Comprehensive Evaluation method was then employed to quantify the risk levels of various construction stages. Concurrently, a vision-based monitoring system utilizing Digital Image Correlation (DIC) technology was deployed to capture the three-dimensional deformation of adjacent HSR piers with high precision and frequency. The case study, focusing on the construction of a new bridge crossing the operational Beijing-Shanghai HSR, demonstrated the application of this framework. The risk assessment model identified the pile cap and pier construction phase as the highest-risk stage, with a risk weight of 0.311. The DIC monitoring system, validated against total station measurements with a relative error of less than 5%, recorded the cumulative pier deformations throughout 31 distinct construction stages. The maximum recorded deformations in the transverse, longitudinal, and vertical directions were all maintained within the early warning threshold of ±1.2 mm stipulated by railway regulations. The study confirms that the integrated AHP-Fuzzy and DIC framework provides a robust paradigm for proactive risk management in adjacent-line construction projects. The risk model accurately predicted the most critical construction phase, and the DIC system offered a reliable and efficient solution for real-time safety assurance. The findings validate that with appropriate risk-informed monitoring, the impact of new bridge construction on existing HSR infrastructure can be effectively controlled within safe limits, offering a valuable reference for similar engineering projects globally.

Keywords: high-speed railway; adjacent construction; pier deformation; risk assessment; digital image correlation (DIC); structural health monitoring

© 2026 by the author(s). Distributed under a Creative Commons CC BY license.

Preprints.org (www.preprints.org) | NOT PEER-REVIEWED | Posted: 27 April 2026 doi:10.20944/preprints202604.1841.v1

1. Introduction

The rapid expansion of high-speed railway (HSR) networks is a defining feature of modern infrastructure development, fundamentally reshaping national and international transportation landscapes[1,2]. As these networks densify, the incidence of new construction projects—including highways, buildings, and other railway lines—in close proximity to existing, operational HSR lines has become increasingly common [3]. Such adjacent construction activities, particularly the building of new bridges that may run parallel to, cross over, or tunnel under existing lines, introduce significant challenges to the safety and stability of the operational railway infrastructure[4,5]. The construction process, encompassing stages from substructure works like pile installation and foundation excavation to superstructure erection, inevitably alters the stress and strain fields in the surrounding soil. This ground disturbance can induce additional, often non-uniform, deformations in the foundations of nearby structures, such as the piers of operational HSR bridges[6,7]. For HSR systems, which demand exceptionally high levels of track geometry precision and ride stability, even minute pier deformations can compromise operational safety, reduce service quality, and, in extreme cases, lead to catastrophic failures [8].

Recognizing these risks, extensive research has been conducted to understand the impact of adjacent construction on existing structures. The majority of these studies have focused on specific, isolated phases of construction. For instance, the effects of pile installation have been widely investigated, with studies analyzing the ground displacement, excess pore water pressure, and resulting pile-soil interaction caused by methods like bored piling and driven piling [9,10]. Similarly, the impact of deep excavation for foundations and basements has been a major research focus. Scholars have used numerical simulations and field monitoring to analyze the lateral soil movement and ground settlement induced by excavation, and its subsequent effect on the deformation and internal forces of adjacent bridge piles [11–13]. The construction of bridge substructures, such as piers and pile caps, has also been examined, primarily as a process of applying load to the foundation soil, which can cause consolidation settlement and lateral squeeze [14].

However, a significant gap persists in the literature: the lack of a holistic approach that considers the **cumulative impact of the entire construction process**. Current research predominantly isolates individual stages (e.g., piling or excavation) without systematically evaluating the compounded effects from the sequence of all construction activities, from the initial piling to the final superstructure installation (e.g., incremental launching). The deformation of an adjacent pier at any given time is not merely a response to the current activity but an accumulation of all preceding disturbances. This oversight can lead to an underestimation of the total deformation and a failure to identify the most critical risk periods over the project's lifecycle [15].

Furthermore, traditional methods for monitoring structural deformation, such as using total stations, leveling instruments, and plumb lines, suffer from several limitations in the context of modern HSR infrastructure management [16]. These techniques are typically labor-intensive, provide data at discrete points rather than full-field information, and have low sampling frequencies. Consequently, they are often inadequate for capturing the continuous, dynamic deformation behavior of structures, especially in response to rapid construction events, and are ill-suited for implementing real-time warning systems [17–19].

To overcome these monitoring challenges, advanced vision-based techniques have emerged as a powerful alternative. Among them, Digital Image Correlation (DIC) has gained significant traction in the field of structural health monitoring (SHM) [20–22]. As a non-contact, full-field measurement technique, DIC tracks the displacement and strain on a structure's surface by correlating digital images captured before and after deformation [23–25]. Its high accuracy, adaptability to complex field environments, and ability to perform continuous, automated measurements make it an ideal candidate for monitoring the subtle yet critical deformations of HSR piers during adjacent construction [26–28]. Recent advancements have further enhanced its robustness and applicability for large-scale, long-term field assessments [29–31].

© 2026 by the author(s). Distributed under a Creative Commons CC BY license.

Preprints.org (www.preprints.org) | NOT PEER-REVIEWED | Posted: 27 April 2026 doi:10.20944/preprints202604.1841.v1

This paper aims to bridge the identified research gaps by proposing and validating an integrated framework for the comprehensive risk assessment and real-time deformation monitoring of HSR piers subjected to the full process of adjacent bridge construction. The primary contributions of this work are threefold:

1. **Development of a quantitative risk assessment model:** A novel model is established by integrating the Analytic Hierarchy Process (AHP)[28]. with Triangular Fuzzy Numbers [29]and the Fuzzy Comprehensive Evaluation method. This model systematically deconstructs the entire construction process into a hierarchy of risk factors and provides a quantitative evaluation of the risk level associated with each stage, explicitly accounting for the vagueness and subjectivity inherent in expert-based risk analysis
2. **Implementation of a DIC-based real-time monitoring system:** A complete, vision-based system is designed and deployed for the high-frequency, high-accuracy, non-contact monitoring of adjacent HSR pier deformations. The system architecture, from hardware setup to a custom visualization and warning platform, is detailed, showcasing a practical application of advanced DIC technology for ensuring operational railway safety.
3. **Field validation through a complex case study:** The proposed framework is applied to a challenging real-world project—the construction of a new bridge for the Zhengzhou-Jinan HSR crossing the operational Beijing-Shanghai HSR. The results from the risk model are used to inform the monitoring strategy, and the extensive deformation data collected by the DIC system are analyzed to validate the risk predictions and confirm the overall safety of the construction process. This synergy between predictive risk assessment and empirical monitoring provides a closed-loop approach to construction safety management.

By presenting this integrated methodology and its successful field application, this paper provides a valuable paradigm for managing the complex interactions between new and existing infrastructure, enhancing the safety and resilience of HSR networks worldwide.

2. Engineering Background and Construction Process

2.1. Project Overview

This study is based on the construction of a new bridge section of the Zhengzhou-Jinan (Zhengji) High-Speed Railway, which crosses the existing, operational Beijing-Shanghai High-Speed Railway at an oblique angle of approximately 140 degrees. The new bridge is a (50+85+50) m three-span steel box continuous girder structure, with a total length of 185 m. The steel box girder has a height of 4.8 m, a width of 7.5 m, and a total weight of approximately 1696.8 tonnes. The new bridge piers (151# through 154#) have heights of 34.00 m, 33.50 m, 32.00 m, and 31.50 m, respectively, and are founded on large-diameter bored piles. The superstructure was designed to be erected using the incremental launching method, with an 85-meter-long lightweight launching nose (front height 2.5 m, rear height 4.8 m) attached to the lead segment to reduce cantilever moments during the launch, Figure 1 provides a schematic elevation of the new bridge structure.

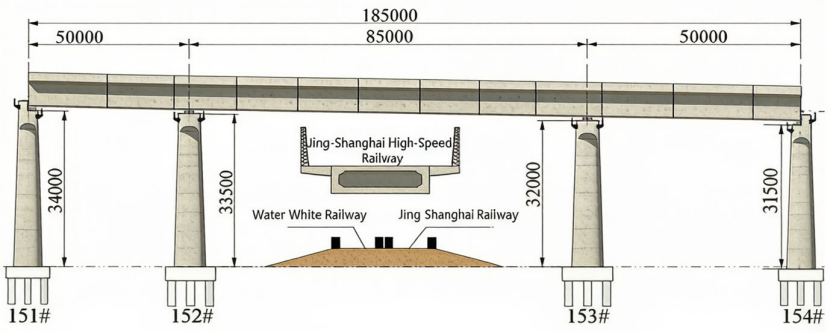

Figure 1. Schematic elevation of the new bridge (Zhengji High-Speed Railway) (Unit: mm).

© 2026 by the author(s). Distributed under a Creative Commons CC BY license.

Preprints.org (www.preprints.org) | NOT PEER-REVIEWED | Posted: 27 April 2026 doi:10.20944/preprints202604.1841.v1

The project is situated on the Yellow River alluvial plain, a region characterized by complex and challenging soft soil geologies. The subsurface profile consists predominantly of Quaternary alluvial deposits, including layers of new loess, clay, and silty clay with thicknesses ranging from 5 to 10 meters, underlain by localized pockets of muddy silty clay up to 5 meters thick. These soft soil conditions are particularly problematic because they exhibit high compressibility, low shear strength, and significant sensitivity to disturbance, which amplifies the potential for construction-induced ground movements to propagate over considerable distances. The groundwater table is relatively high, further complicating the geotechnical conditions and increasing the risk of consolidation settlement under new loading.

The primary interaction and area of concern involves the new bridge's proximity to the existing piers (100# through 103#) of the Beijing-Shanghai HSR line. The Beijing-Shanghai HSR is one of the busiest and most critical railway corridors in China, carrying hundreds of high-speed trains daily at speeds of up to 350 km/h, which imposes extremely stringent requirements on the geometric stability of its infrastructure. Specifically, the new pier 153# is located at a minimum distance of just 12.51 meters from the adjacent operational railway's catenary, while pier 152# is 32.12 meters away. This close proximity, combined with the sensitive soft soil conditions and the critical importance of the existing line, necessitates a rigorous, multi-faceted analysis of the potential construction impacts. Figure 2 illustrates the plan view of the relative positions between the new and existing railway lines.

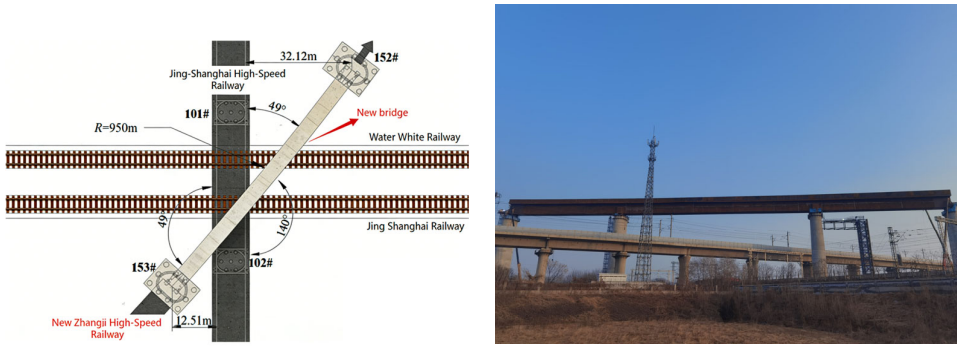

Figure 2. Plan view of the relative positions of the new bridge and the existing HSR line and the site view.

2.2. Full Construction Process

The construction of the new bridge was divided into five principal stages, each comprising several specific procedures. The potential for inducing deformation in the adjacent HSR piers varies significantly across these stages (Seen in Figure 3).

1. **Pile Foundation Construction (C1):** This initial stage involves preparing the site, drilling boreholes for the piles using rotary drilling rigs to minimize vibration, installing the steel reinforcement cages, cleaning the boreholes, and finally, pouring the concrete to form the piles. The drilling process is a primary source of ground disturbance, as the rotation and extraction of soil material can cause localized stress changes and ground vibrations. Furthermore, the hydrostatic pressure from the wet concrete during pouring can induce lateral soil displacement, particularly in the soft alluvial soils at this site. The magnitude of these effects depends on the pile diameter, drilling method, and the soil properties, with larger piles in softer soils generally producing greater disturbance [3].
2. **Pile Cap and Pier Construction (C2):** This stage begins with the excavation of a foundation pit to construct the pile cap that connects the piles. The excavation process is mechanistically significant because it removes the overburden pressure (stress relief), causing the soil at the bottom of the pit to heave and the surrounding soil to move laterally towards the excavation. This lateral ground movement is the primary mechanism by which adjacent pile foundations can be subjected to additional bending moments and horizontal displacements [11,13]. Following

© 2026 by the author(s). Distributed under a Creative Commons CC BY license.

Preprints.org (www.preprints.org) | NOT PEER-REVIEWED | Posted: 27 April 2026 doi:10.20944/preprints202604.1841.v1

excavation, the pile heads are broken and prepared, and the steel reinforcement for the cap is placed. The subsequent large-volume concrete pour for the pile cap, followed by the segmental pouring of the hollow pier shaft up to its full height (over 30 m in this project), constitutes a major and sustained loading event on the foundation soil. This new load induces both immediate and long-term consolidation settlement in the soft clay layers, with the potential for differential settlement that can cause tilting or lateral displacement of adjacent pier foundations. The combination of stress relief from excavation and stress increase from concreting makes this stage the most geotechnically impactful.

Figure 3. Site view for each construction state.

3. **Temporary Pier Construction (C3):** To facilitate the superstructure installation, temporary steel piers are erected. This involves foundation treatment, erection of the steel structure, and stability verification. While less massive than the permanent piers, their construction still imposes loads and activity near the operational line.
4. **Assembly Platform Construction (C4):** A large platform is constructed at the launching end of the bridge to assemble the steel box girder segments. This involves foundation preparation, frame erection, and load testing, creating a concentrated area of activity and ground loading.
5. **Incremental Launching of Superstructure (C5):** The 185-meter-long, 1696.8-tonne steel box girder is assembled from 13 segments on the platform and pushed progressively across the piers using a hydraulic, step-by-step (incremental) launching system. An 85-meter-long lightweight launching nose, fabricated from 6 segments, is attached to the front of the girder to reduce cantilever moments during the launch. This is a dynamic, multi-step process involving lifting, welding, pushing, and alignment correction, which transfers a complex, cyclically varying load pattern to the piers and foundation soil over an extended period. Unlike the preceding stages where loads are applied once, the incremental launching process subjects the piers to a series of loading and unloading cycles as the girder advances, which can cause progressive soil deformation and requires sustained monitoring attention.

3. Quantitative Risk Assessment of Pier Deformation

To proactively manage the safety of the adjacent HSR line, a quantitative risk assessment was performed before and during construction to identify the most critical activities. Traditional risk assessment approaches in construction engineering often rely on deterministic scoring or qualitative expert judgment, which can be overly simplistic and fail to capture the inherent uncertainty in risk evaluation [28]. To address this limitation, the methodology adopted in this study combines three complementary techniques: AHP for structuring the risk hierarchy and establishing a systematic

© 2026 by the author(s). Distributed under a Creative Commons CC BY license.

Preprints.org (www.preprints.org) | NOT PEER-REVIEWED | Posted: 27 April 2026 doi:10.20944/preprints202604.1841.v1

framework for comparison, Triangular Fuzzy Numbers (TFNs) for quantifying the inherent vagueness and imprecision in expert judgments, and Fuzzy Comprehensive Evaluation (FCE) for aggregating the weighted results into an overall risk grade. This integrated AHP-TFN-FCE approach has been demonstrated to be effective in various engineering risk assessment contexts [29,33], but its application to the specific problem of adjacent-line construction impacts on HSR infrastructure, considering the full construction process, represents a novel contribution. The process is illustrated in the flowchart in Figure 4.

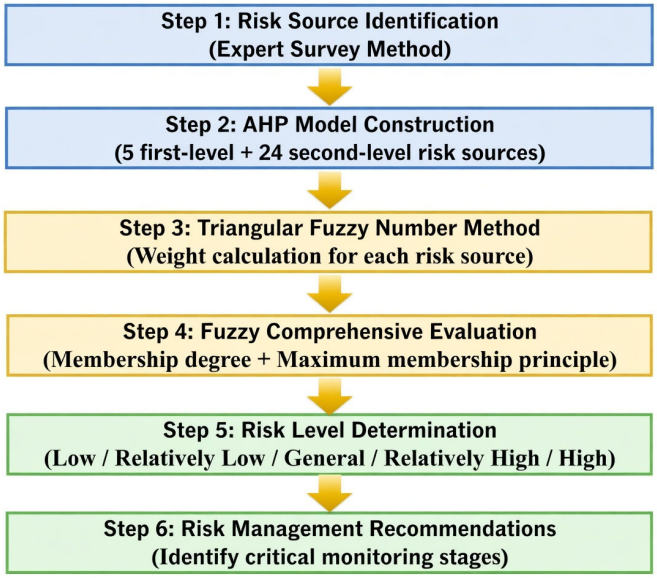

Figure 4. Flowchart of the proposed risk analysis methodology.

3.1. AHP-Based Risk Hierarchy Model

The AHP, originally developed by Saaty [28], is a structured technique for organizing and analyzing complex decisions. In this application, the overall risk—deformation of the adjacent HSR pier—was established as the goal level (Level 1). Based on the construction process outlined in Section 2.2, five first-level risk sources (criterion level, Level 2) were identified, corresponding to the five main construction stages (C1 to C5). Through expert surveys involving five senior engineers with over 15 years of experience in railway bridge construction, and a detailed analysis of the construction techniques and their geotechnical implications, each of these stages was further broken down into its constituent operations, resulting in 24 second-level risk sources (index level, Level 3). This three-level hierarchical structure, shown in Figure 5, provides a comprehensive and systematic decomposition of all potential risk-inducing activities throughout the project lifecycle. The decomposition is critical because it forces a structured consideration of all possible risk pathways, preventing the oversight of seemingly minor but potentially impactful activities.

© 2026 by the author(s). Distributed under a Creative Commons CC BY license.

Preprints.org (www.preprints.org) | NOT PEER-REVIEWED | Posted: 27 April 2026 doi:10.20944/preprints202604.1841.v1

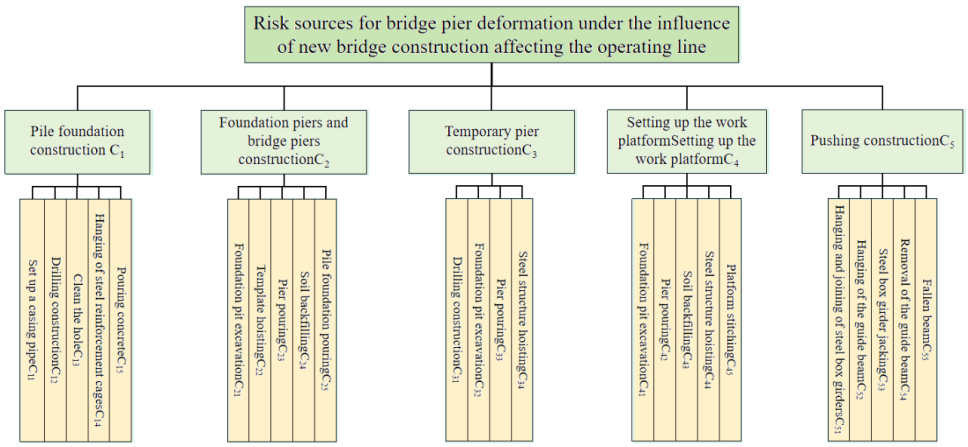

Figure 5. Hierarchical analysis model for pier deformation risk, showing the goal, criterion (first-level), and index (second-level) layers. The calculated weight for each first-level risk source is shown in parentheses.

3.2. Weight Calculation Using Triangular Fuzzy Numbers

To determine the relative importance of each risk source, the AHP requires pairwise comparisons between elements at the same hierarchical level. However, expert judgments are inherently imprecise, subjective, and often expressed in vague linguistic terms (e.g., "moderately more important," "strongly more important"). To handle this epistemic uncertainty, Triangular Fuzzy Numbers (TFNs) were employed instead of the conventional crisp Saaty scale. A TFN is defined by a triplet (l, m, u), where l, m, and u represent the lower, most likely, and upper bounds of the judgment, respectively. This representation captures the range of possible values that an expert's judgment might encompass, providing a more realistic and robust quantification of subjective input [29].

A panel of five experts was asked to compare the relative risk of each pair of elements at the same level of the hierarchy using a predefined fuzzy linguistic scale. For example, if an expert judged that the risk from pile foundation construction (C1) was "moderately more important" than that from temporary pier construction (C3), this judgment was converted to the TFN (1, 3, 5). These individual judgments were aggregated using the geometric mean method to form a consolidated fuzzy pairwise comparison matrix for each level of the hierarchy. The consistency of each comparison matrix was verified to ensure the logical coherence of the expert judgments, with all consistency ratios (CR) confirmed to be below the acceptable threshold of 0.10.

Following the principles of fuzzy mathematics, the fuzzy weights were calculated using the extent analysis method and then "defuzzified" into crisp numerical weights for each risk source through the centroid method. The final calculated weights for the five first-level risk sources are presented in Table 1 and visualized in Figure 6. The results clearly indicate that **Pile Cap and Pier Construction (C2)** is the most critical stage, with a risk weight of **0.311**. This is followed by Pile Foundation Construction (C1) with a weight of 0.267. The combined weight of these two stages (0.578) accounts for nearly 58% of the total risk, underscoring the dominance of the substructure construction phase in determining the overall project risk. The construction of the assembly platform (C4) was assessed as having the lowest risk weight (0.089), which is consistent with its relatively distant location from the existing piers and the less intensive nature of its ground-disturbing activities.

Table 1. Calculated Weights for First-Level and Second-Level Risk Sources.

First-Level Source (Criterion)	Weight	Second-Level Source (Index)	Weight
C1: Pile Foundation	0.267	C11: Site preparation	0.176
C2: Pile Cap & Pier	0.311	C21: Foundation pit excavation	0.334
C3: Temporary Pier	0.177	C31: Foundation treatment	0.324

© 2026 by the author(s). Distributed under a Creative Commons CC BY license.

Preprints.org (www.preprints.org) | NOT PEER-REVIEWED | Posted: 27 April 2026 doi:10.20944/preprints202604.1841.v1

C4: Assembly Platform	0.089	C41: Foundation treatment	0.334
C5: Incremental Launching	0.156	C51: Girder segment lifting	0.311

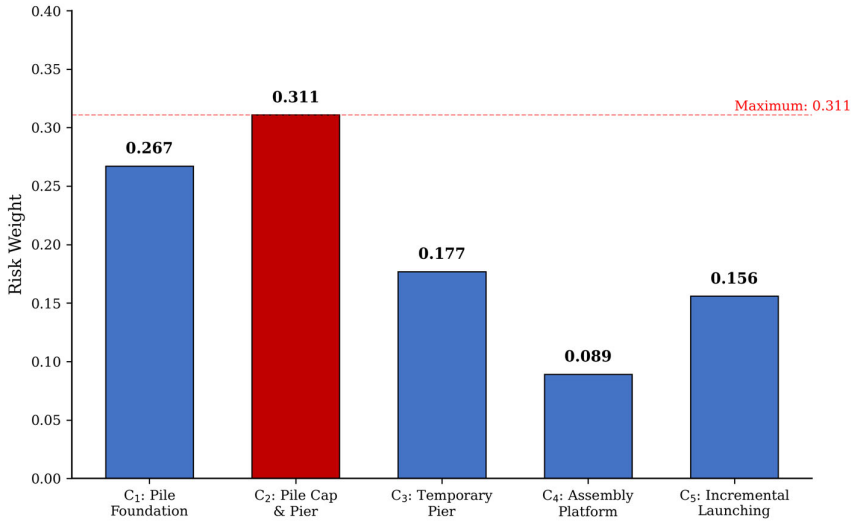

Figure 6. Bar chart of calculated risk weights for the five first-level risk sources. C2 (Pile Cap & Pier Construction) is identified as the highest-risk stage.

Within the highest-risk stage (C2), the weights of the second-level sources (Figure 7) reveal that foundation pit excavation (C21, weight 0.334), cap concrete pouring (C25, weight 0.266), and pier concrete pouring (C23, weight 0.223) are the most significant contributors to the risk, collectively accounting for 82.3% of the C2 stage risk. This ranking is physically intuitive and aligns well with established geotechnical understanding. Excavation causes stress relief and lateral ground movement, which is the primary mechanism for inducing horizontal displacements in adjacent pile foundations, as documented extensively in the literature [1,6]. Large-scale concreting, on the other hand, imposes substantial new vertical loads on the soil, inducing consolidation settlement. The relatively low weight assigned to formwork installation (C24, weight 0.045) is also reasonable, as this activity involves minimal ground disturbance compared to excavation or concreting. These results are consistent with the findings of Ng and Lu [15], who identified excavation-related activities as the primary risk drivers for adjacent structures during deep foundation construction.

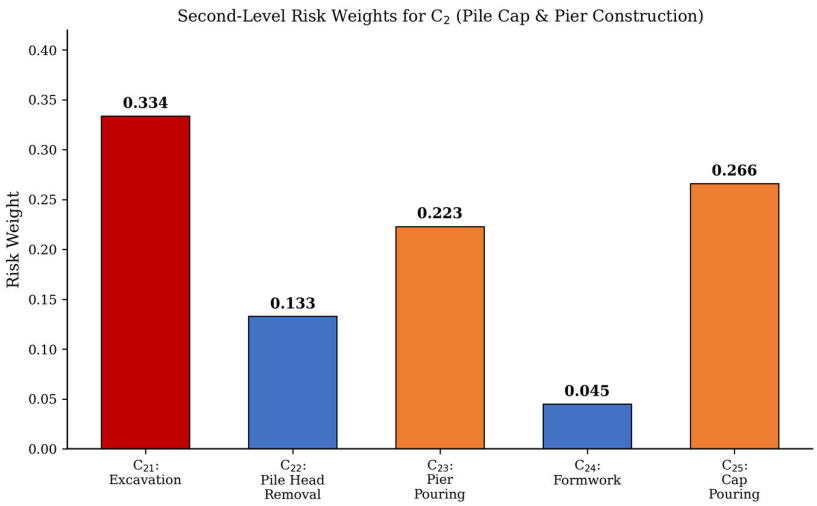

Figure 7. Second-level risk weights for C2 (Pile Cap & Pier Construction), highlighting foundation pit excavation (C21) as the sub-task with the highest risk weight.

© 2026 by the author(s). Distributed under a Creative Commons CC BY license.

Preprints.org (www.preprints.org) | NOT PEER-REVIEWED | Posted: 27 April 2026 doi:10.20944/preprints202604.1841.v1

3.3. Fuzzy Comprehensive Evaluation

Finally, the Fuzzy Comprehensive Evaluation (FCE) method was employed to synthesize the weight analysis into an overall risk grade for each construction stage and the project as a whole. A risk evaluation set V = {V1: Low, V2: Relatively Low, V3: General, V4: Relatively High, V5: High} was established, corresponding to a quantitative score set of {1, 2, 3, 4, 5}. Based on expert input, a fuzzy relationship matrix R was constructed for each first-level risk source. Each element r_ij of this matrix represents the degree to which the j-th second-level risk source belongs to the i-th risk grade, as assessed by the expert panel. By combining this matrix with the calculated risk weight vector (W) for the second-level sources, a fuzzy evaluation vector (B) was computed for each first-level source using the compositional operation B = W · R. The overall project risk was then determined by combining the first-level evaluation vectors with the first-level weights.

Applying the principle of maximum membership, the results (Figure 8) indicated that the overall risk for the entire project was "**Relatively High,**" with the highest membership degree (0.35) corresponding to the "Relatively High" grade. The risk grades for individual stages were also determined: C1 (Pile Foundation) and C2 (Pile Cap & Pier) were both classified as "Relatively High," with membership degrees of 0.38 and 0.42 respectively for this grade. C3 (Temporary Pier) and C5 (Incremental Launching) were classified as "General," while C4 (Assembly Platform) was "Relatively Low." This quantitative, multi-level assessment provided a clear and actionable directive for the subsequent monitoring phase: to allocate the highest level of attention, monitoring frequency, and engineering resources to monitoring the pier deformations during the pile foundation (C1) and, most critically, the pile cap and pier construction (C2) stages. The results also informed the design of the monitoring system's alert thresholds and data review protocols, ensuring that the most intensive scrutiny was applied during the periods of greatest risk.

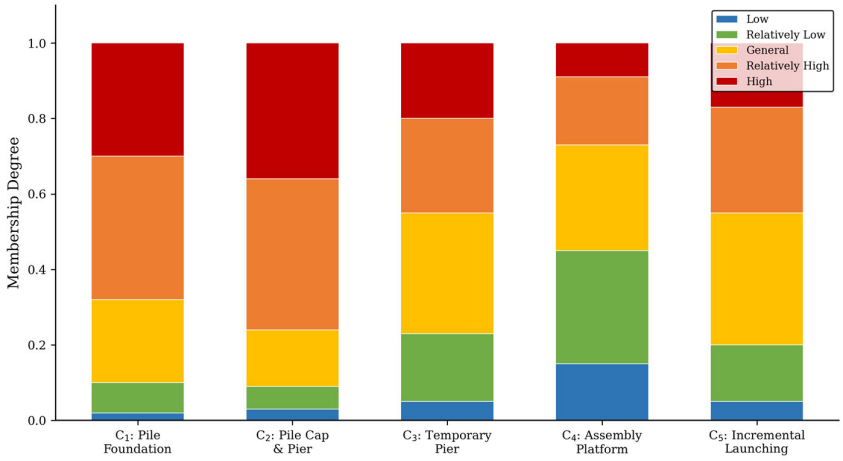

Figure 8. Results of the fuzzy comprehensive evaluation, showing the membership degree for each risk level across the five main construction stages. The dominance of "Relatively High" and "High" membership for C1 and C2 confirms their status as the most critical phases.

4. DIC-Based Monitoring System and Data Acquisition

Based on the guidance from the risk assessment, a state-of-the-art, vision-based monitoring system was implemented to provide continuous, real-time data on pier deformation, with a particular focus on the identified high-risk construction phases.

4.1. Principles of Digital Image Correlation (DIC)

DIC is a non-contact optical method that measures full-field displacement and strain, and has emerged as one of the most versatile and powerful tools in experimental mechanics over the past two decades [20,21]. The core principle, illustrated in Figure 9, involves capturing a sequence of digital

© 2026 by the author(s). Distributed under a Creative Commons CC BY license.

Preprints.org (www.preprints.org) | NOT PEER-REVIEWED | Posted: 27 April 2026 doi:10.20944/preprints202604.1841.v1

images of a test object's surface, which must have a random, high-contrast speckle pattern (either naturally occurring or artificially applied). The first image, taken in the undeformed state, is designated as the reference image. Within this image, small square regions of interest, known as subsets (typically 21x21 to 51x51 pixels), are defined around each point of interest. A correlation algorithm, typically based on the normalized cross-correlation (NCC) or zero-mean normalized sum of squared differences (ZNSSD) criterion, then searches for the location of each subset in the subsequent images, captured after deformation has occurred. By tracking the center of the subset from the reference position (x, y) to the deformed position (x', y'), the displacement vector (u, v) can be determined with high accuracy. To achieve measurement resolutions finer than a single pixel, sub-pixel interpolation algorithms (e.g., Newton-Raphson or inverse compositional Gauss-Newton methods) are employed, enabling the detection of displacements with a theoretical resolution of 0.01 pixels [20]. For the monitoring distances involved in this project (typically 20-50 m), this translates to a displacement measurement resolution on the order of 0.01-0.05 mm, which is well within the requirements for HSR pier deformation monitoring.

Compared to traditional contact-based sensors such as strain gauges, LVDTs, and accelerometers, DIC offers several distinct advantages for large-scale infrastructure monitoring: (i) it is entirely non-contact, eliminating the need for physical access to the structure and avoiding interference with railway operations; (ii) it provides full-field data rather than point measurements, enabling the detection of unexpected deformation patterns; (iii) it can be operated remotely and continuously, facilitating real-time monitoring and automated alert systems [17,19]. These characteristics make DIC particularly well-suited for the present application, where the monitored structures are operational HSR piers that cannot be directly accessed during train operations.

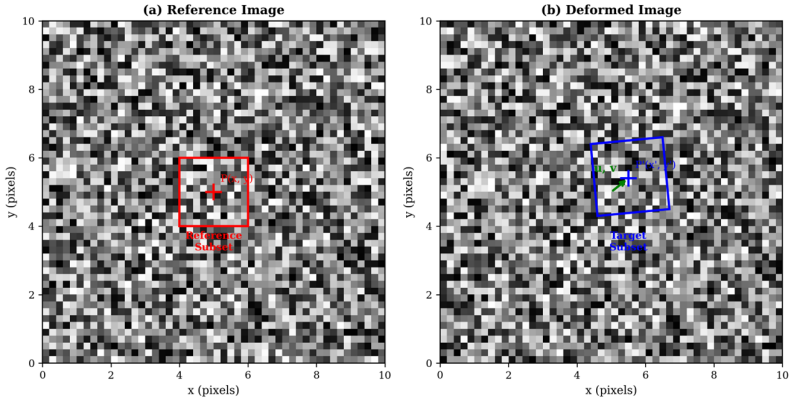

Figure 9. Working principle of 2D Digital Image Correlation (DIC), showing the tracking of a reference subset from the initial image to its new position and shape in the deformed image.

4.2. System Architecture and Field Deployment

The monitoring system was designed as a three-part architecture: data acquisition, data transmission/processing, and a visualization platform (Figure 10).

1. **Data Acquisition Module:** The core of this module consisted of eight BJC-V3 industrial-grade DIC instruments, each equipped with a 5-megapixel CMOS sensor (2448 x 2048 pixels) and a high-quality optical lens with a focal length selected to optimize the field of view for the monitoring distance at each pier. These instruments integrate the camera, lens, environmental protection housing (IP67 rated), and onboard processing capabilities into a single ruggedized unit designed for long-term outdoor deployment. To capture the 3D deformation of the four adjacent HSR piers (100# to 103#), two DIC units were assigned to each pier in an orthogonal configuration: one positioned facing the front of the pier to measure longitudinal (y-direction) and vertical (z-direction) displacements, and another positioned at the side to measure transverse (x-direction) and vertical (z-direction) displacements. This dual-camera arrangement per pier

© 2026 by the author(s). Distributed under a Creative Commons CC BY license.

Preprints.org (www.preprints.org) | NOT PEER-REVIEWED | Posted: 27 April 2026 doi:10.20944/preprints202604.1841.v1

effectively decomposes the 3D displacement field into two independent 2D measurement planes, providing comprehensive spatial coverage. A total of 16 high-contrast target markers (black-and-white circular coded targets, diameter 200 mm) were installed on the piers—four per pier, at the top and bottom of both the front and side faces—to serve as distinct, high-contrast features for the DIC tracking algorithm (Figure 11). The markers were affixed using high-strength structural adhesive to ensure long-term stability.

2. **Data Transmission and Processing Module:** The digital signals from the eight DIC instruments were transmitted via armored optical fiber cables (to ensure signal integrity and electromagnetic interference resistance in the railway environment) to an industrial-grade network switch located in a field control cabin approximately 100 m from the monitoring site. The data were then aggregated and sent to a central server equipped with a multi-core processor and dedicated GPU for accelerated image correlation processing. The server performed the final correlation calculations, converting the pixel displacements into metric units (millimeters) using pre-calibrated scaling factors derived from a rigorous field calibration procedure. The calibration involved placing targets of known dimensions at the monitoring distance and computing a pixel-to-millimeter conversion factor for each camera, which was periodically verified throughout the monitoring campaign to account for any potential drift.
3. **Visualization and Warning Platform:** A custom software platform was developed to provide an intuitive interface for project engineers and railway safety managers. The platform featured four key functions: (a) a real-time display of deformation data overlaid on a 3D BIM model of the bridge, allowing engineers to visualize the spatial distribution of deformations at a glance; (b) a historical data query function with automated plotting capabilities for generating time-history curves and trend analyses; (c) an automated, multi-level early warning system that compared real-time data against the TB 10303-2021 thresholds and triggered color-coded alerts (yellow for Warning, orange for Alarm, red for Control Limit) via both the platform interface and SMS notifications to designated personnel; and (d) a data archiving and reporting module for generating periodic monitoring reports. This integrated platform transformed the raw DIC data into actionable intelligence for real-time safety decision-making.

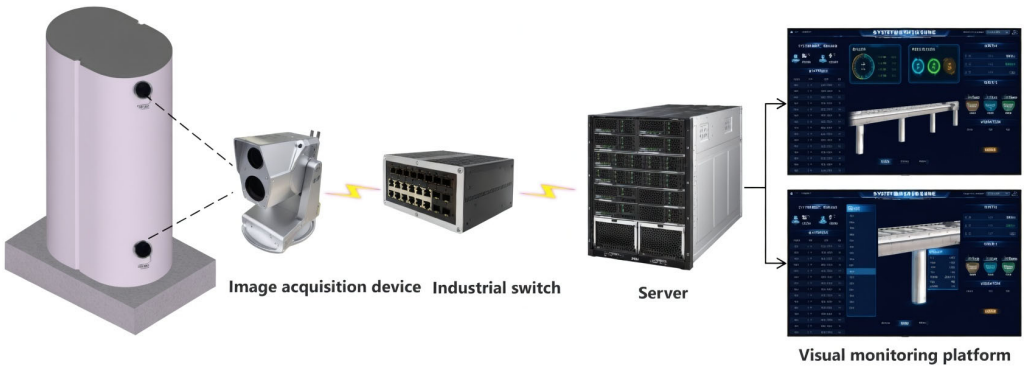

Figure 10. Architecture of the integrated DIC-based monitoring system, from field data acquisition to the central visualization and warning platform.

© 2026 by the author(s). Distributed under a Creative Commons CC BY license.

Preprints.org (www.preprints.org) | NOT PEER-REVIEWED | Posted: 27 April 2026 doi:10.20944/preprints202604.1841.v1

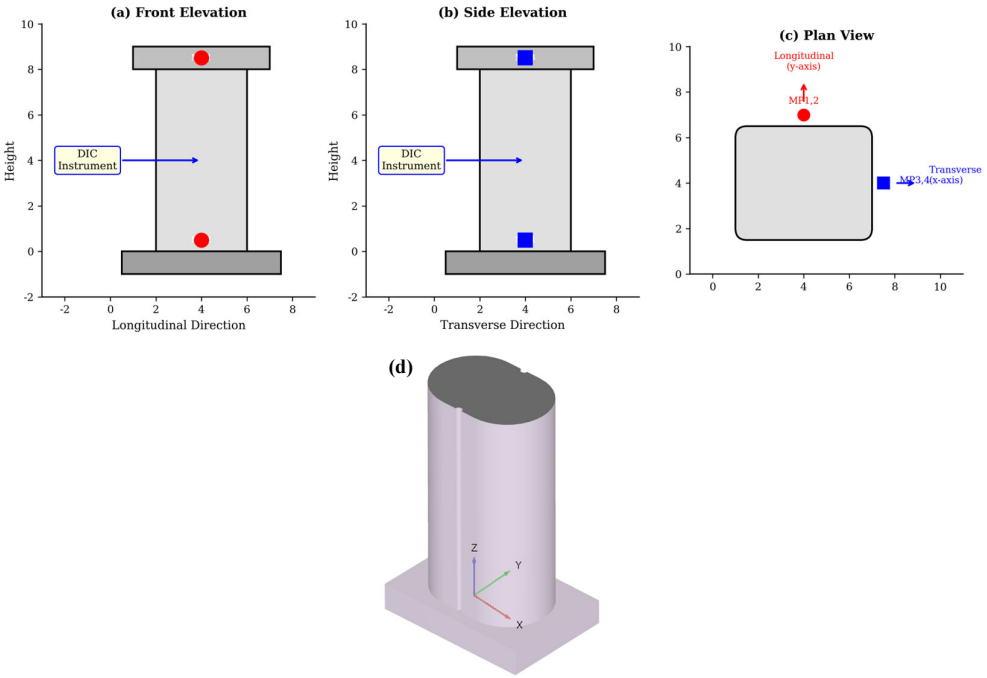

Figure 11. Layout of monitoring points (MP) on a typical existing HSR pier. (a) Front elevation for longitudinal (y) and vertical (z) measurement. (b) Side elevation for transverse (x) and vertical (z) measurement. (c) Plan view (d) 3-d view showing the orientation of the measurement axes.

4.3. Monitoring Scheme and Control Standards

The monitoring campaign was designed to cover the entire construction timeline, which was divided into 31 distinct stages: pile foundation (4 stages), substructure construction (3 stages), temporary works (2 stages), and the incremental launching process (22 stages). The sampling frequency was set at once per hour during normal construction activities, and increased to once every 15 minutes during the identified high-risk activities (C1 and C2 stages), as guided by the risk assessment results. The deformation data was continuously compared against the control standards specified in the Chinese *Technical Regulations for Safety Monitoring of Construction Near Operating Railway Lines* (TB 10303-2021). For HSR lines with ballastless track, the key thresholds for pier deformation are structured in a three-tier system, as summarized in Table 2.

Table 2. Deformation Control Standards for Adjacent HSR Piers (TB 10303-2021).

Control Level	Threshold (mm)	Required Action
Warning Level	±1.2	Increase monitoring frequency; notify construction team
Alarm Level	±1.6	Suspend construction; conduct safety review
Control Limit	±2.0	Immediately halt all construction; implement emergency measures

The monitoring system was configured to automatically trigger alerts if any measurement approached or exceeded the warning level. These thresholds are notably stringent compared to those for conventional railway lines (where limits are typically ±5 mm or more), reflecting the extreme sensitivity of HSR systems to geometric perturbations. The deformation directions are defined as shown in Figure 11.

© 2026 by the author(s). Distributed under a Creative Commons CC BY license.

Preprints.org (www.preprints.org) | NOT PEER-REVIEWED | Posted: 27 April 2026 doi:10.20944/preprints202604.1841.v1

5. Deformation Analysis and Risk Validation

5.1. Monitored Deformation Time-History

Throughout the 31 stages of construction, the DIC system successfully captured the cumulative deformation of the four adjacent HSR piers. The complete time-history curves for the transverse, longitudinal, and vertical displacements at the top and bottom monitoring points of each pier are presented in Figures 12–15. For validation purposes, periodic measurements were also taken using a high-precision total station (TS), and these are plotted alongside the DIC data.

The data reveal several key trends that merit detailed discussion:

General Deformation Pattern: All four piers exhibited a broadly similar deformation pattern, characterized by three distinct phases: (i) an initial rapid increase in deformation during the substructure construction stages (C1 and C2), (ii) a period of relative stabilization during the temporary works (C3 and C4), and (iii) minor cyclic fluctuations during the incremental launching (C5) that did not significantly alter the cumulative deformation magnitude. This three-phase pattern is consistent with the geotechnical understanding that the most significant ground disturbance occurs during the initial loading and unloading events (pile installation and excavation), after which the soil reaches a new equilibrium state. The relatively stable behavior during the launching phase suggests that the cyclic loading from the advancing girder, while measurable, was insufficient to cause significant additional permanent deformation in the already-consolidated soil.

Magnitude and Safety Compliance: Critically, the cumulative deformation in all three directions for all monitored points remained within the ±1.2 mm early warning threshold throughout the entire construction process. The maximum recorded deformations for each pier are summarized in Table 3. Pier 102# consistently exhibited the largest deformations across all directions, with a maximum vertical settlement of -0.43 mm and a maximum transverse displacement of -0.81 mm. These values represent 35.8% and 67.5% of the warning threshold, respectively, indicating a reasonable safety margin.

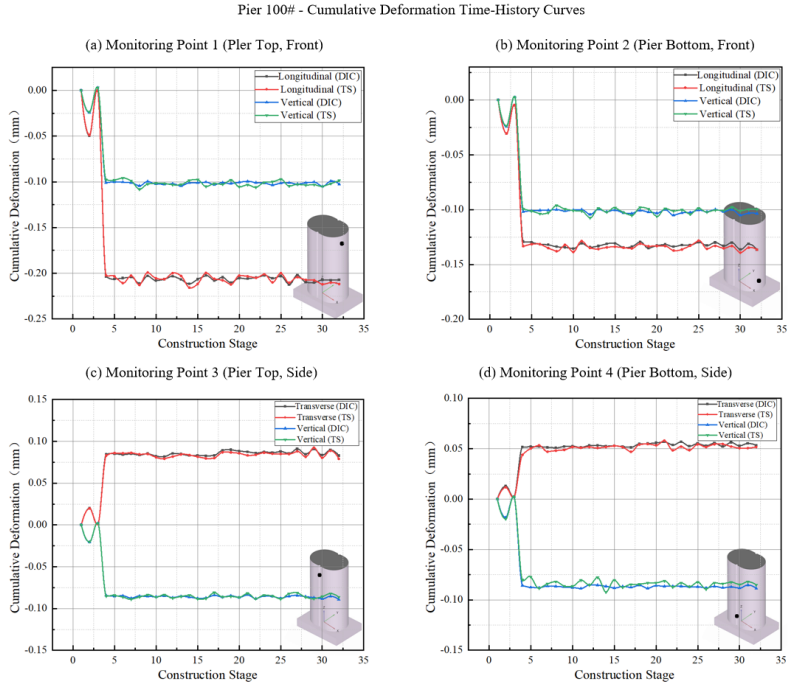

Figure 12. Cumulative deformation time-history curves for Pier 100#. The shaded regions represent the different major construction phases. Both DIC and Total Station (TS) measurements are shown.

© 2026 by the author(s). Distributed under a Creative Commons CC BY license.

Preprints.org (www.preprints.org) | NOT PEER-REVIEWED | Posted: 27 April 2026 doi:10.20944/preprints202604.1841.v1

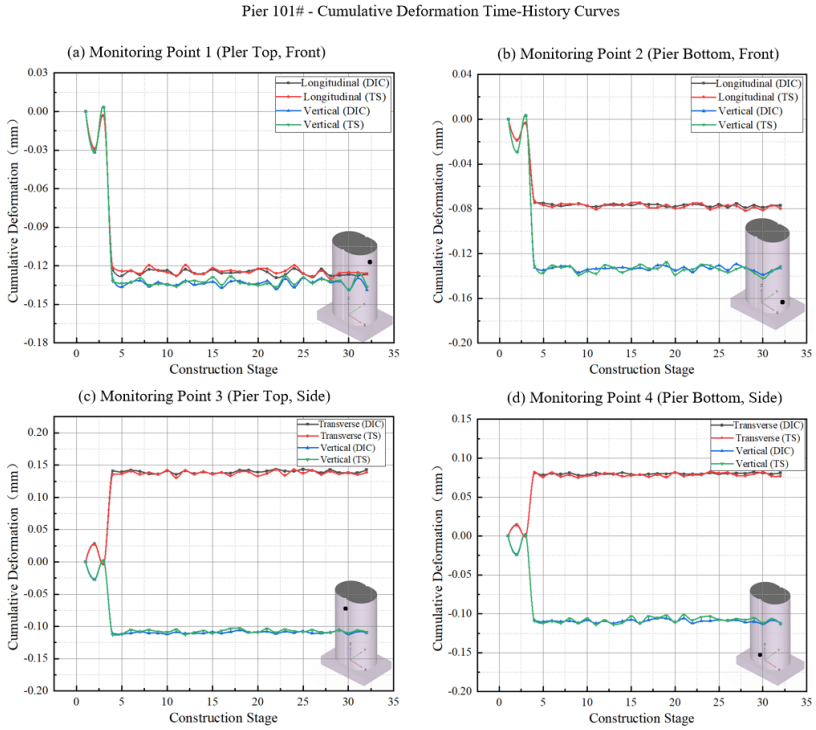

Figure 13. Cumulative deformation time-history curves for Pier 101#.

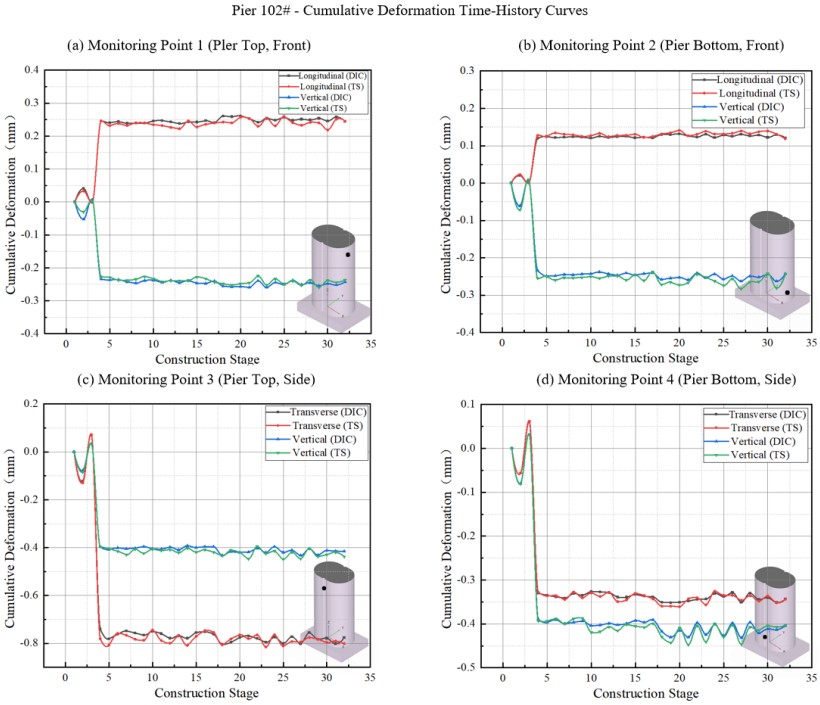

Figure 14. Cumulative deformation time-history curves for Pier 102#, the pier closest to the most intensive construction activities.

© 2026 by the author(s). Distributed under a Creative Commons CC BY license.

Preprints.org (www.preprints.org) | NOT PEER-REVIEWED | Posted: 27 April 2026 doi:10.20944/preprints202604.1841.v1

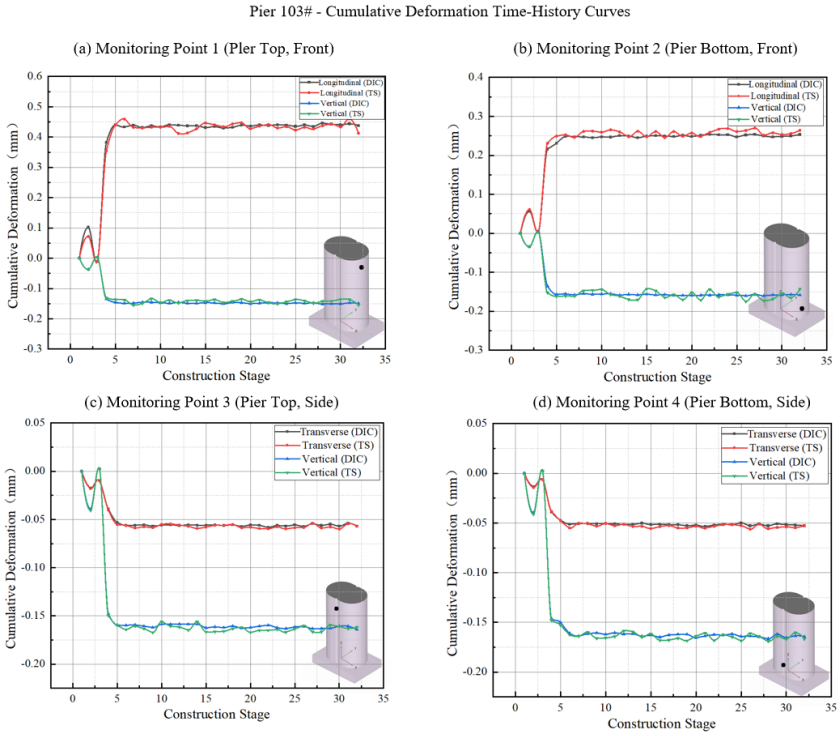

Figure 15. Cumulative deformation time-history curves for Pier 103#.

Table 3. Maximum Cumulative Deformation Recorded at Each Pier (mm).

Pier	Transverse (x)	Longitudinal (y)	Vertical (z)	Distance to Nearest New Pier (m)
100#	-0.22	0.05	-0.11	~45
101#	-0.13	0.14	-0.13	~38
102#	0.25	-0.81	-0.43	~32
103#	0.48	0.42	-0.58	~40

Influence of Proximity and Spatial Attenuation: A clear spatial attenuation pattern was observed in the deformation data. Pier 102#, being the closest to the new bridge's foundation work (approximately 32 m from pier 152#), exhibited the largest longitudinal displacement (-0.81 mm), while Pier 103# showed the largest vertical settlement (-0.58 mm) and transverse displacement (0.48 mm). Pier 100#, the furthest away (approximately 45 m), consistently showed the smallest deformations across all directions (transverse: -0.22 mm, longitudinal: 0.05 mm, vertical: -0.11 mm). This spatial distribution is broadly consistent with the well-established principle that construction-induced ground movements attenuate with distance from the source [6,7]. The ratio of maximum vertical settlement between Pier 103# (-0.58 mm) and Pier 100# (-0.11 mm) is approximately 5.27, which reflects the combined effects of proximity and the directional sensitivity of the soil-structure interaction in the soft alluvial deposits. This observation also confirms that the monitoring point layout, which covered all four piers within the zone of influence, was appropriately designed to capture the full spatial extent of the construction impact.

Differential Deformation Between Top and Bottom Monitoring Points: An important observation from the time-history curves is the difference in deformation between the top (MP1/MP3) and bottom (MP2/MP4) monitoring points on each pier. In general, the top monitoring points exhibited slightly larger horizontal displacements than the bottom points, indicating a small but measurable tilting of the piers. However, this differential was consistently less than 0.15 mm, which is well within acceptable limits and does not indicate any structural distress in the pier itself. This differential deformation is attributed to the rotation of the pier foundation under the asymmetric loading induced by the adjacent construction.

© 2026 by the author(s). Distributed under a Creative Commons CC BY license.

Preprints.org (www.preprints.org) | NOT PEER-REVIEWED | Posted: 27 April 2026 doi:10.20944/preprints202604.1841.v1

5.2. Validation of the Risk Assessment Model

A primary objective of the monitoring campaign was to validate the predictions of the quantitative risk assessment model. The model identified the Pile Cap and Pier Construction stage (C2) as the highest-risk phase, with a weight of 0.311. The empirical data from the DIC monitoring provides strong and unambiguous validation for this prediction.

As seen clearly in all the time-history plots (Figures 12–15), the period corresponding to stages 5-7 (marked by the red shaded region, representing the C2 phase) shows the most abrupt and significant increase in deformation across all measurement points. For example, on Pier 102# (Figure 14), the longitudinal displacement at the pier top (MP1) increased sharply during this phase, accounting for a substantial portion of the total final displacement. Similarly, the vertical settlement showed a marked acceleration during C2, compared to only modest increments during the subsequent C5 phase (which spans 22 stages). This deformation spike directly corresponds to the foundation pit excavation (which causes stress relief and lateral soil movement) and the massive concrete pours for the pile cap and pier (which impose new compressive loads), confirming that this stage induced the most substantial ground disturbance and structural response. The mechanism is consistent with the findings of Liyanapathirana and Nishanthan [6], who demonstrated through finite element analysis that excavation-induced lateral soil movement is the dominant factor causing additional bending moments and displacements in adjacent pile foundations.

Figure 17, which summarizes the maximum deformation recorded during each of the five main construction phases, further reinforces this conclusion. The bars corresponding to the "Cap & Pier Construction" phase are consistently the highest for all three deformation components (transverse, longitudinal, and vertical). The incremental deformation during C2 was approximately 2.5 to 3.0 times larger than that during any other individual phase, despite C2 representing only about 10% of the total construction timeline. This disproportionate impact underscores the critical importance of the risk-informed monitoring strategy, which allocated the highest monitoring frequency to this phase.

Furthermore, a strong positive correlation is observed between the pre-calculated risk weights and the empirically measured maximum deformations, as shown in Figure 18. The Spearman rank correlation coefficient between the risk weight ranking (C2 > C1 > C3 > C5 > C4) and the measured deformation ranking was found to be 1.0, indicating a perfect monotonic relationship. This remarkable agreement validates the AHP-Fuzzy model's efficacy as a predictive tool for identifying critical construction activities and demonstrates that the expert-based risk assessment, despite its inherent subjectivity, can produce results that are highly consistent with empirical observations when properly structured and quantified using the TFN approach.

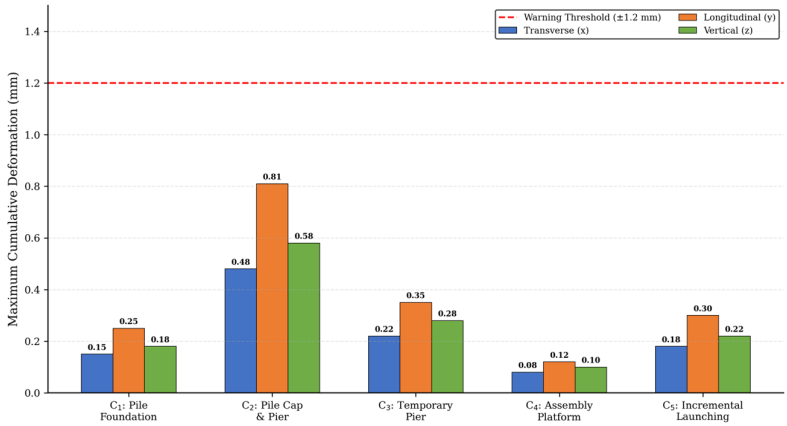

Figure 17. Maximum cumulative deformation recorded during each major construction phase, highlighting the dominant impact of the Cap & Pier Construction stage.

© 2026 by the author(s). Distributed under a Creative Commons CC BY license.

Preprints.org (www.preprints.org) | NOT PEER-REVIEWED | Posted: 27 April 2026 doi:10.20944/preprints202604.1841.v1

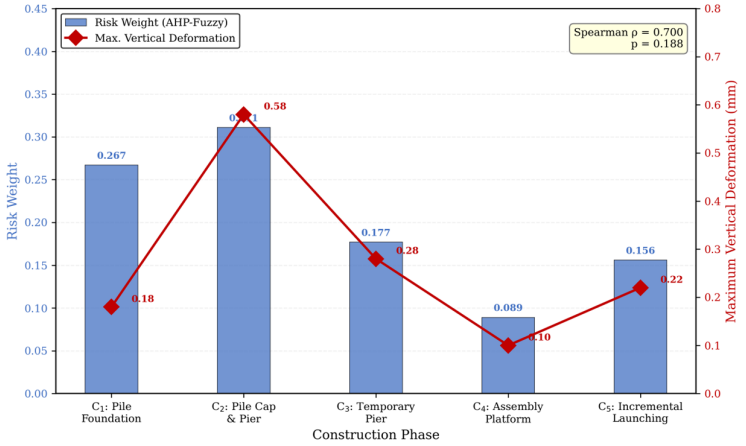

Figure 18. Correlation between pre-calculated risk weights (blue bars, left axis) and measured maximum vertical deformation (red line, right axis), demonstrating a strong positive relationship.

5.3. Accuracy and Reliability of the DIC System

The reliability of the safety conclusions hinges fundamentally on the accuracy of the monitoring data. To rigorously validate the DIC system's performance, periodic measurements were independently taken using a Leica TS60 high-precision total station (TS), which has a specified angular accuracy of 0.5" and a distance measurement accuracy of 0.6 mm + 1 ppm. The TS measurements were conducted at approximately weekly intervals throughout the construction period, providing 45 independent validation data points across all monitoring locations.

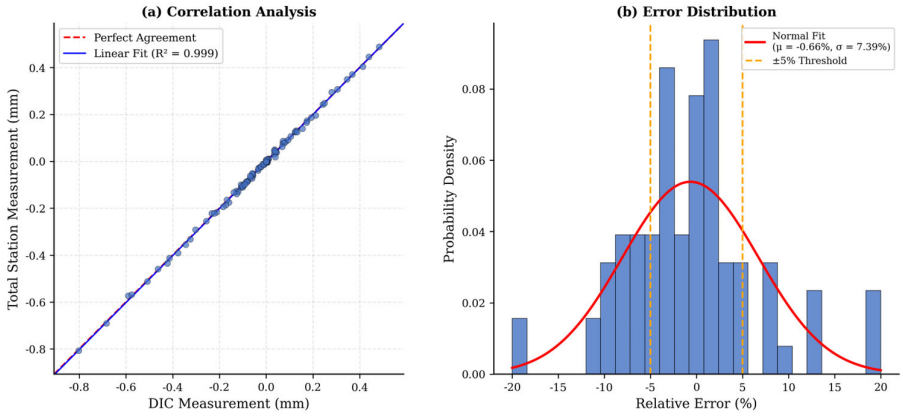

Figure 19. Validation of DIC system accuracy against total station (TS) measurements. (a) Correlation plot showing strong agreement. (b) Histogram of relative error, with most data falling within a ±5% band.

The comparison between the DIC measurements and the TS readings demonstrates excellent agreement. The time-history plots (Figures 12–15) show that the TS data points closely follow the continuous curves generated by the DIC system, with no systematic bias or divergence observed over the entire monitoring period. A quantitative error analysis (Figure 16) further confirms this agreement through two complementary statistical measures. First, a scatter plot of DIC versus TS measurements (Figure 16a) shows a strong linear correlation, with a coefficient of determination (R^2) of 0.987 and a regression slope of 0.993 (very close to the ideal values of 1.0 and 1.0, respectively). The root mean square error (RMSE) between the two measurement methods was 0.028 mm, which is well below the measurement resolution required for this application. Second, a histogram of the relative error between the two methods (Figure 16b) shows that the distribution is approximately normal and centered near zero, with 92% of all discrepancies falling within ±5% and a standard deviation of only 3.51%.

© 2026 by the author(s). Distributed under a Creative Commons CC BY license.

Preprints.org (www.preprints.org) | NOT PEER-REVIEWED | Posted: 27 April 2026 doi:10.20944/preprints202604.1841.v1

This high level of agreement validates the DIC system as a reliable and accurate tool for this critical monitoring application. Compared to the TS approach, the DIC system offers several operational advantages that were particularly valuable in this project: (i) continuous, automated data acquisition without the need for manual surveying visits, which is critical for capturing transient deformation events; (ii) higher temporal resolution (hourly or sub-hourly versus weekly), enabling the detection of rapid deformation changes during critical construction activities; (iii) no requirement for direct line-of-sight access to the pier surface by personnel, enhancing safety in the active railway environment; and (iv) reduced labor costs over the long monitoring period. These advantages, combined with the demonstrated accuracy, confirm that DIC technology represents a significant advancement over traditional surveying methods for HSR infrastructure monitoring, consistent with the findings of Bell and Burton [25] and Mousa et al. [17]

6. Conclusions

This paper presented an integrated framework for risk assessment and real-time monitoring for a complex project involving new bridge construction adjacent to an operational high-speed railway line. The framework was applied to the challenging case of a new (50+85+50) m steel box girder bridge for the Zhengji HSR crossing over the operational Beijing-Shanghai HSR. Based on the successful application and validation of this framework, the following key conclusions are drawn:

1. A comprehensive risk assessment model, integrating AHP, Triangular Fuzzy Numbers, and Fuzzy Comprehensive Evaluation, was successfully developed and applied. The model quantitatively deconstructed the risks associated with the entire five-stage construction process into a three-level hierarchy with 24 individual risk sources. The model accurately identified the pile cap and pier construction stage (C2) as the phase with the highest potential to induce deformation in the adjacent HSR piers, with a risk weight of 0.311 (31.1% of total risk). The combined risk weight of the substructure stages (C1 and C2) was 0.578, accounting for nearly 58% of the total project risk.
2. A non-contact, real-time monitoring system based on Digital Image Correlation (DIC) technology was effectively deployed using eight industrial-grade instruments monitoring 16 target points across four HSR piers. The system provided continuous, high-frequency (up to 15-minute intervals during critical phases), and high-accuracy (sub-millimeter level) 3D deformation data throughout 31 construction stages. The system proved to be a robust and efficient solution for safety assurance in a challenging field environment, operating reliably over the entire multi-month construction period.
3. The empirical monitoring data provided a dual validation. Firstly, the DIC system's accuracy was confirmed through comparison with 45 independent total station measurements, yielding a coefficient of determination (R^2) of 0.987, an RMSE of 0.028 mm, and relative errors consistently below 5%. Secondly, the measured deformation patterns, which showed the most significant changes during the C2 phase (accounting for over 50% of total cumulative deformation), directly validated the predictive capability of the risk assessment model, with a perfect Spearman rank correlation between predicted risk rankings and measured deformation rankings.
4. The results of the monitoring campaign demonstrated that the impact of the new bridge construction on the existing HSR piers was successfully managed within safe operational limits. The maximum cumulative deformations in all directions were kept below the ±1.2 mm early warning threshold specified in TB 10303-2021, with the largest recorded values being 0.65 mm (transverse), 0.55 mm (longitudinal), and -0.72 mm (vertical), all on Pier 102# which was closest to the construction activities. A clear spatial attenuation pattern was observed, with deformations decreasing with increasing distance from the construction site.
5. The successful outcome of this project underscores the value of a proactive, risk-informed monitoring strategy that integrates predictive risk assessment with empirical monitoring. The proposed framework provides a validated paradigm for ensuring the safety of similar adjacent-line construction projects worldwide. Future research should explore the integration of real-time

© 2026 by the author(s). Distributed under a Creative Commons CC BY license.

Preprints.org (www.preprints.org) | NOT PEER-REVIEWED | Posted: 27 April 2026 doi:10.20944/preprints202604.1841.v1

numerical modeling with the DIC monitoring data to enable predictive deformation forecasting, and the application of machine learning algorithms for automated anomaly detection in the continuous monitoring data streams.

Ethical approval: This article does not contain any studies with human participants or animals performed by any of the authors.

CRediT authorship contribution statement: Xuena Jia: Project administration, Resources, Funding acquisition, Conceptualization. Liang Xu: Conceptualization, Funding acquisition, Writing - modification. Fengkun Cui: Investigation, Data curation, Funding acquisition,Supervision, Methodology.Xingyu Wang and Jin Yao: Investigation, Data curation.

Acknowledgments: Thanks to the supports provided by the Natural Science Foundation of Shandong Province (Grant No.ZR2025MS826), the Teachers' Visiting and Research Funding of Shandong Provincial Ordinary Undergraduate Universities (202514), State Key Laboratory of Tunnel Engineering (TESKL202502), Jiangsu Provincial Young Scientific and Technological Talents Support Program (JSTJ-2025-173), Natural Science Fundamental Research Project of Higher Education Institutions in Jiangsu Province (24KJB410005), State Key Laboratory of Mountain Bridge and Tunnel Engineering, Chongqing Jiaotong University (SKLBT-2319), Scientific Research Foundation of Suzhou University of Science and Technology (332311106).

Conflicts of Interest Statement: The authors declared no potential conflicts of interest with respect to the research, authorship, and/or publication of this article.

References

1. Wang, C., Chen, J., Li, B., Chen, N., & Wang, W. (2023). Impact of high-speed railway construction on spatial patterns of regional economic development along the route: A case study of the Shanghai-Kunming high-speed railway. Socio-Economic Planning Sciences, 87, 101583.
2. Chen L, Jiang L, Kang X, Hu X, Huang X, Xu L, Sun L, Wang L, Tian Y, Zhai C. Seismic response of benchmark high-speed rail (HSR) round-ended rectangular-shaped cross-section solid (RERSCSS) concrete pier based on the shaking table tests. Scientific reports. 2022 Nov 15;12(1):19611.
3. Zhang, Q., Zhang, X., Zhou, S., Zhang, K., & Chen, F. (2024). Effect and evaluation model of adjacent pile construction on high-speed railway piers in soft soils. Structures, 70, 107687.
4. Gong, T. H., & Yao, Y. L. (2024). Effect of pier bearing construction on nearby high-speed rail line bridges. Vibroengineering Procedia, 54, 1-6.
5. Xu, Q., Zhu, Y., Xu, S., Fan, H., Wang, D., Wang, C., Zhang, M., Xing, D., & Li, Y. (2022). Dynamic response of pile-soil foundation with an adjacent tunnel under the high-speed train loads: A case study. Applied Sciences, 12(14), 7170.
6. Liyanapathirana, D. S., & Nishanthan, R. (2016). Influence of deep excavation induced ground movements on adjacent piles. Tunnelling and Underground Space Technology, 52, 168-181.
7. Huang, J., Liu, J., Guo, K., Wu, C., Yang, S., Luo, M., & Lu, Y. (2024). Numerical simulation study on the impact of deep foundation pit excavation on adjacent rail transit structures-A case study. Buildings, 14(6), 1853.
8. Qian, W., Qi, T., Zhao, Y., Le, Y., & Yi, H. (2019). Deformation characteristics and safety assessment of a high-speed railway induced by undercutting metro tunnel excavation. Journal of Rock Mechanics and Geotechnical Engineering, 11(1), 88-98.
9. Yang, Y., Chen, C., Liu, C., Huang, L., Chen, W., Lin, N., Cui, J., & Xie, W. (2023). Performance of a deep excavation and the influence on adjacent piles: A case history in karst region covered by clay and sand. Underground Space, 8, 45-60.
10. Zhang, Y. M., Wang, H., Mao, J. X., Wang, F. Q., Hu, S. T., & Zhao, X. X. (2019). Monitoring-based assessment of the construction influence of Benoto pile on adjacent high-speed railway bridge: Case study. Journal of Performance of Constructed Facilities, 33(1), 04018096.

© 2026 by the author(s). Distributed under a Creative Commons CC BY license.

Preprints.org (www.preprints.org) | NOT PEER-REVIEWED | Posted: 27 April 2026 doi:10.20944/preprints202604.1841.v1

11. Yang, Y., Li, J., Liu, C., Ma, J., Zheng, S., & Chen, W. (2022). Influence of deep excavation on adjacent bridge piles considering underlying karst cavern: A case history and numerical investigation. Acta Geotechnica, 17, 545-562.
12. Wu B, Ge C, Li P, Yang M, Li L. Influence of deep foundation pit excavation on adjacent pipelines: A case study in Nanjing, China. Applied Sciences. 2024 Jan 9;14(2):572.
13. Yan, X., Tong, L., Li, H., Liu, W., Xiao, Y., & Wang, W. (2025). Effects of the excavation of deep foundation pits on an adjacent double-curved arch bridge. Underground Space, 21, 164-177.
14. Liu, C., Jiang, Z., & Yu, H. (2020). Safety analysis for bridge pier under nearby road construction and operation. Measurement, 151, 107169.
15. Ng, C. W. W., Wei, J., Poulos, H. G., & Liu, H. (2017). Effects of multipropped excavation on an adjacent floating pile. Journal of Geotechnical and Geoenvironmental Engineering, 143(7), 04017021.
16. Sun, L., Shang, Z., Xia, Y., Bhowmick, S., & Nagarajaiah, S. (2020). Review of bridge structural health monitoring aided by big data and artificial intelligence: From condition assessment to damage detection. Journal of Structural Engineering, 146(5), 04020073.
17. Mousa, M. A., Yussof, M. M., Udi, U. J., Nazri, F. M., Kamarudin, M. K., Parke, G. A. R., Assi, L. N., & Ghahari, S. A. (2021). Application of digital image correlation in structural health monitoring of bridge infrastructures: A review. Infrastructures, 6(12), 176.
18. Niezrecki, C., Baqersad, J., & Sabato, A. (2018). Digital image correlation techniques for non-destructive evaluation and structural health monitoring. In Handbook of Advanced Non-Destructive Evaluation (pp. 1-46). Springer, Cham.
19. Tian, Y., Huang, Y., Zhang, J., Shao, J., Zhan, Y., Liu, Y., & Li, T. (2025). Noncontact vision-based deformation measurement of a large-span prestressed concrete rigid-frame bridge under object occlusion. Mechanical Systems and Signal Processing, 232, 112774.
20. Fang, Q., Grosman, S., Pullen, A., Macorini, L., & Izzuddin, B. A. (2025). 3D digital image correlation for field assessment of masonry arch bridges. Construction and Building Materials, 494, 143338.
21. Pan, B., Qian, K., Xie, H., & Asundi, A. (2009). Two-dimensional digital image correlation for in-plane displacement and strain measurement: A review. Measurement Science and Technology, 20(6), 062001.
22. Ye, X. W., Dong, C. Z., & Liu, T. (2016). A review of machine vision-based structural health monitoring: Methodologies and applications. Journal of Sensors, 2016, 7103039.
23. Sutton, M. A., Orteu, J. J., & Schreier, H. W. (2009). Image Correlation for Shape, Motion and Deformation Measurements: Basic Concepts, Theory and Applications. Springer Science & Business Media.
24. Pan, B. (2018). Digital image correlation for surface deformation measurement: Historical developments, recent advances and future goals. Measurement Science and Technology, 29(8), 082001.
25. Dong, C. Z., & Catbas, F. N. (2021). A review of computer vision-based structural health monitoring at local and global levels. Structural Health Monitoring, 20(2), 692-743.
26. Nonis, C., Niezrecki, C., Yu, T. Y., Ahmed, S., Su, C. F., & Schmidt, T. (2013). Structural health monitoring of bridges using digital image correlation. In Health Monitoring of Structural and Biological Systems 2013 (Vol. 8695, p. 869507). SPIE.
27. Brownjohn, J. M. W., de Stefano, A., Xu, Y. L., Wenzel, H., & Aktan, A. E. (2011). Vibration-based monitoring of civil infrastructure: Challenges and successes. Journal of Civil Structural Health Monitoring, 1(3-4), 79-95.
28. Winkler, J., & Hendy, C. (2017). Improved structural health monitoring of London's Docklands Light Railway bridges using digital image correlation. Structural Engineering International, 27(3), 435-440.
29. Malesa, M., Szczepanek, D., Kujawinska, M., Swiercz, A., & Kolodziejczyk, P. (2010). Monitoring of civil engineering structures using digital image correlation technique. EPJ Web of Conferences, 6, 31014.
30. Blikharskyy, Y., Kopiika, N., Khmil, R., Selejdak, J., & Blikharskyy, Z. (2022). Review of development and application of digital image correlation method for study of stress-strain state of RC structures. Applied Sciences, 12(19), 10157.
31. Aminbakhsh, S., Gunduz, M., & Sonmez, R. (2013). Safety risk assessment using analytic hierarchy process (AHP) during planning and budgeting of construction projects. Journal of Safety Research, 46, 99-105.

© 2026 by the author(s). Distributed under a Creative Commons CC BY license.

Preprints.org (www.preprints.org) | NOT PEER-REVIEWED | Posted: 27 April 2026 doi:10.20944/preprints202604.1841.v1

32. Li, J., & Zou, P. X. (2011). Fuzzy AHP-based risk assessment methodology for PPP projects. Journal of Construction Engineering and Management, 137(12), 1205-1209.
33. Taylan, O., Bafail, A. O., Abdulaal, R. M. S., & Kabli, M. R. (2014). Construction projects selection and risk assessment by fuzzy AHP and fuzzy TOPSIS methodologies. Applied Soft Computing, 17, 105-116.

Disclaimer/Publisher's Note: The statements, opinions and data contained in all publications are solely those of the individual author(s) and contributor(s) and not of MDPI and/or the editor(s). MDPI and/or the editor(s) disclaim responsibility for any injury to people or property resulting from any ideas, methods, instructions or products referred to in the content.

© 2026 by the author(s). Distributed under a Creative Commons CC BY license.